A study of a coasting easterly wave

By T. N. KRISHNAMURTI[1] and MASAO KANAMITSU[1], *Department of Meteorology, Florida State University, Tallahassee, Florida, U.S.A.*

(Manuscript received August 21, 1972; revised version May 3, 1973)

ABSTRACT

An application of a multi-level primitive equation model is presented here. The model physics include air-sea interaction, shallow and deep moist convection and long-wave radiative effects. An example of a prediction for a nondeveloping easterly wave is presented in this paper. It is shown that it is possible to obtain a reasonable prediction of the motion and intensity of the wave up to periods of around 72 hours. The calculations are extended to examine a number of important relevant topics such as: (i) the maintenance and energetics of the cold core disturbance, (ii) the restoring mechanism on the large-scale conditional instability of the tropical atmosphere during and after disturbance passage, (iii) the effects of differential long-wave radiation on the prediction, (iv) statistical equilibrium of the area of parameterized cumulus scale motions as a function of the larger scale motions, and (v) the importance of a simple parameterization procedure for short range prediction.

I. Introdution

This study deals with the numerical prediction of a non-developing easterly wave. Besides the usual questions of forecast verification and reasonable specifications of convective rainfall we are also concernned with a number of other questions that deal with the following topics.

(i) Practical validity of a simple cumulus parameterization procedure, where the vertical distribution of heating is determined from a moist static energy conservation principle. Our scheme is discussed in Krishnamurti et al. (1973).

(ii) On the restoring of large-scale conditional instability over the tropics.

(iii) The maintenance of the cold low, and its energetics.

(iv) Statistical equilibrium of the area occupied by deep convection.

It has been possible to expand this study into these enquiries because of a stable and somewhat reasonable numerical prediction of the large-scale dependent variables. The details of the prediction model are given in the previous paper, hereafter referred to as I.

[1] Work completed while on visit to the National Center for Atmospheric Research which is sponsored by the National Science Foundation.

Besides the conventional surface network and ship observations, there were roughly 40 upper air stations in our domain between 108° W to 42° W and 6° N to 34° N. This was supplemented by one level of aircraft Doppler wind data. A grid size of 2° latitude by 2° longitude was used in the numerical integrations.

The weather situation at the initial time consists of the following features (see Baumhefner, 1968, for details of maps for OOZ 13 August 1961).

(*a*) The lower tropospheric easterly wave is located over the Carribbean. The wave axis is around the eastern part of Cuba.

(*b*) Maximum wave amplitude is found around 700 mb.

(*c*) A cold core thermal structure is found below 700 mb and a warm core above 700 mb was noted in the observations. The temperature amplitude of the wave was around 1.5°C.

(*d*) The axis of a mid-oceanic cold-core upper trough with coldest temperatures around 300 mb and strong winds near 200 mb was located over central Cuba. The axis of this upper trough had a strong tilt from southwest to northeast.

The lower tropospheric easterly wave was observed to move westward at a speed of roughly 6° longitude/day. The wave did not amplify into a hurricane, its amplitude at 700

Table 1. *A list of useful symbols*

p	Pressure
z	Geopotential height of constant pressure surface
T	Temperature
q	Specific humidity
H_S	Sensible heat flux from the ocean
L	Latent heat of vaporization
E_B	Evaporation from sea to air
H_R	Rate of radiative warming per unit mass of air
E_m	Moist static energy
Γ_m	Moist static stability
subscript s	Saturation condition
θ_e	Equivalent potential temperature
k^1	Total eddy kinetic energy over a domain
k_z	Zonal kinetic energy
$\langle K_z K_E \rangle$	Exchange of zonal to eddy kinetic energy
$\langle P_E K_E \rangle$	Exchange of eddy available potential energy to eddy kinetic energy

mb was noted to remain nearly invarient for 72 hours. There was active convection to the east of the wave axis, which was noted to propagate westward with the wave. The speed of westward propagation of the lower tropospheric wave was faster than that of the upper cold low. The latter moved westward at a speed of around 2° longitude/day. These two systems were not very strongly coupled during the 72-hour period of interest here. One of the first studies that we conducted was a simple barotropic prediction of the wave at 800 mb. The wave decreased in amplitude by about 60% within 36 hours. The reasons for this became apparent from the energetics, i.e., eddy kinetic energy in the domain was being transferred to zonal kinetic energy. Thus it became quite clear that in order to understand the steady westward propagation of the wave a more sophisticated numerical model is desirable.

2. Quality of prediction of coasting ceasterly wave

Because of sparsity of tropical data we do not feel that the state of forecast verification has quite reached the stage for a detailed statistical evaluation (such as an evaluation of detailed root mean square errors for the individual dependent variables). Nevertheless, we show that the results presented are quite promising and do indeed verify against observations in some detail.

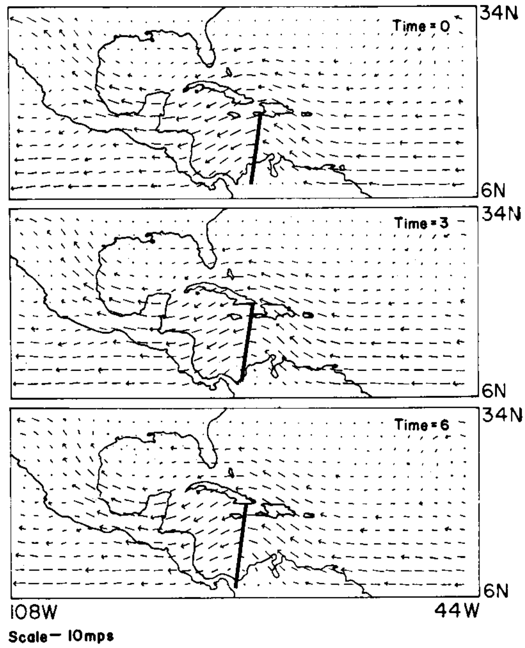

Fig. 2.1. Wind vectors at hours 0, 3 and 6 at 800 mb. Heavy line shows wave axis as determined from relative vorticity maximum at 800 mb.

(*a*) *Motion of the wave at 800 mb*

The maximum intensity of the observed wave was noted around 700 mb. The nearest relevant level where wind field is available for our primitive equation model is a 800 mb

Selected drawings showing the predicted progression of the easterly wave at the 800 mb surface is shown in Figs. 2.1 through 2.4 from time $t = 0$ to time $t = 72$ hours. The slanted line oriented from south to north is the location of the wave axis; this line is determined from the relative vorticity maxima at the 800 mb surface. The largest speeds of the wave are around 20 knots at this level from the east. One notices an essential westward propagation in near steady state for both the amplitude and the speed of motion of the wave during the 72 hour period. The wave moves roughly 7° longitude per day westward. The remarkable stability of the computations in predicting the steady coasting easterly wave has been due to a major improvement of our model. A slight southwest to north-

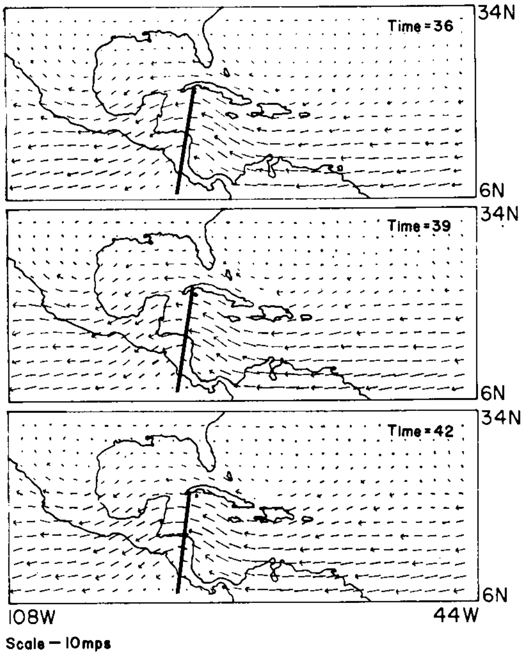

Fig. 2.2. Wind vectors at hours 36, 39 and 42 at 800 mb. Heavy line shows wave axis as determined from relative vorticity maximum at 800 mb.

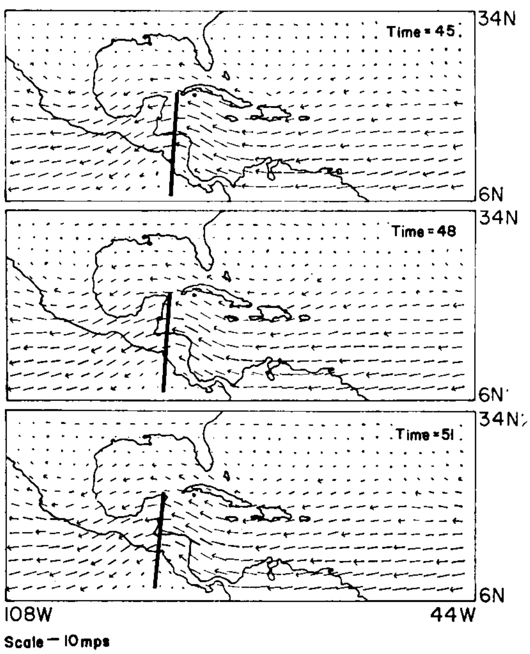

Fig. 2.3. Wind vectors at hours 45, 48 and 51 at 800 mb. Heavy line shows wave axis as determined from relative vorticity maximum at 800 mb.

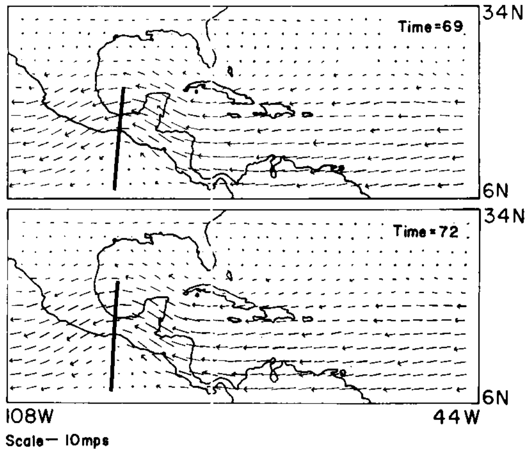

Fig. 2.4. Wind vectors at hours 69 and 72 at 800 mb. Heavy line shows wave axis as determined from relative vorticity maximum at 800 mb.

east tilt was noticed during the entire course of the integration period although this tilt was somewhat less as time progressed towards the 72 hour period. The flow away from the easterly wave in the low latitudes is essentially due east. Fig. 2.5 shows the observed versus forecast wave positions. Phase errors are indeed very small for the first 48 hours. The mean error is of the order of 1.3° longitude/day during the 72 hours.

(*b*) *Vertical motion and convection*

Fig. 2.6 shows an aircraft track between Kingston, Jamaica and Keywest-Florida. This was a low-level observational flight in the sub-cloud layer made between 32 and 38 hour of the

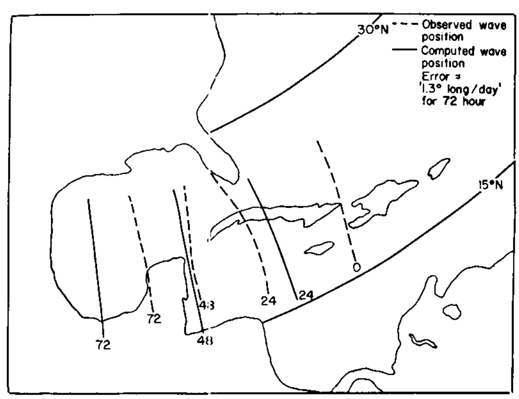

Fig. 2.5. Observed (700 mb) versus forecast (800 mb) position of wave.

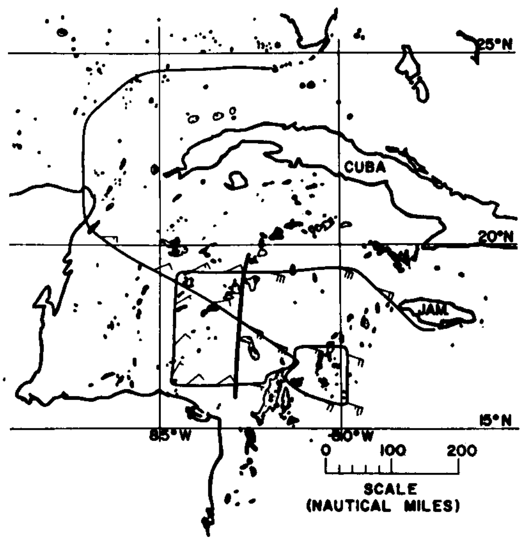

Fig. 2.6. Subcloud layer aircraft track showing low-level observed winds, radar echoes and wave axis. Observations are valid between 32 and 38 hours (This drawing was loaned by Dr W. M. Gray of Colorado State University.)

forecast time. Of interest in these observations are the following features:

(*a*) Location of the easterly wave axis.

(*b*) A wind shift across the wave axis,

(*c*) Location of active convection mostly to the east of the wave axis. Krishnamurti (1968) has discussed these observations. The hard echoes occupy roughly 1 to 2% of the grid-scale area. Some mesoscale bands, essentially oriented south-southwest to north-northeast, may be noted in this drawing. The spacing between these bands is of the order of 2.5° latitude, and with our present grid resolution of 2° latitude the smallest wave that can be resolved would be of the order of 4° latitude. At best we expect to see a computation of vertical motion on the large-scale that has some skill in specifying the overall region of convection behind the wave axis. Indeed computations do bear this out. In Fig. 2.7 we show the distribution of vertical motion at 900 mb at 48 hours of forecast time. The overall agreement between the region of rising motion, on top of the boundary layer, and the observed convection may be noted. The location of the observed wave axis, Fig. 2.7, compares very well with the forecast position at 48 hours, Fig. 2.3. In section 5 we present calculations of the area of deep convection, here

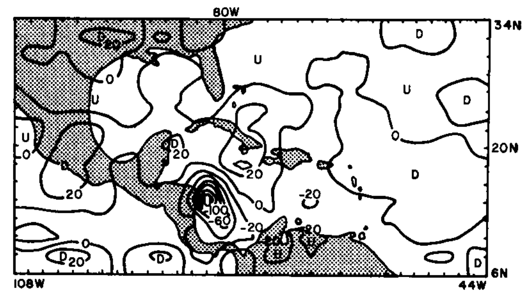

Fig. 2.7. Vertical motion, ω in units 10^{-5} mb/sec, at 900 mb, $t = 48$ hours.

we may note that at 36 hours the predicted region of deep convection (Fig. 5.2) again agrees quite well with observations of hard echoes (Fig. 2.6). The intensity of large-scale vertical motion is around 100 mb/day. As the forecast proceeds toward 72 hours the vertical motion pattern moves westward with the wave.

Vertical motion in a primitive equation prediction model is evaluated from the mass continuity equation. In our model $\omega = 0$ at $p = 100$ mbs and we integrate down to 1 000 mbs, Krishnamurti et al. (1973).

(c) *Westward propagation of moisture front*

During the course of the integration we noted a dry region ahead cf the easterly wave. This dry region was especially pronounced at 700 mb. In this region specific humidities were around 3 g/kg as against 9 g/kg behind the wave. Although the initial data in the Caribbean

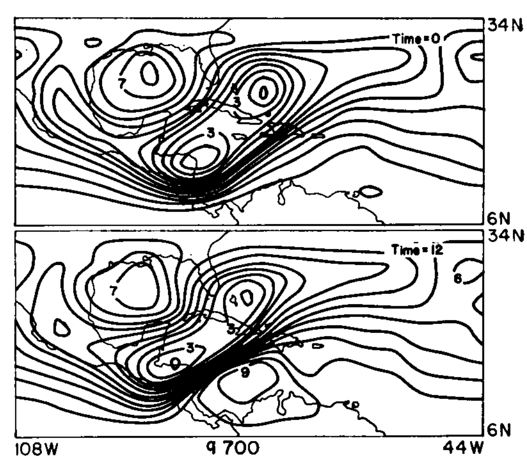

Fig. 2.8. Specific humidity at 700 mb, units g/k, for hours $t = 0$ and $t = 12$.

37 – 732899

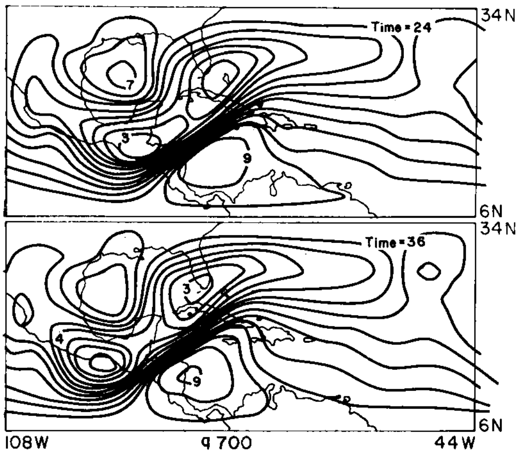

Fig. 2.9. Specific humidity at 700 mb, units g/kg, for hours $t = 24$ and $t = 36$.

was not quite adequate to resolve this phenomenon of the moisture front adequately, the forecast fields after 12 hours through 72 hours show this very clearly. These are shown in Figs. 2.8 through 2.11.

Observations at 36 hours do confirm the existence of a very sharp moisture front. These were published by Krishnamurti (1968) and Baumhefner (1968). It should be noted that there is no corresponding front-like feature in the temperature field or even in the virtual temperature field. In this experiment the maintenance of the moisture front is primarily attributed to dynamic descending motions ahead of the easterly

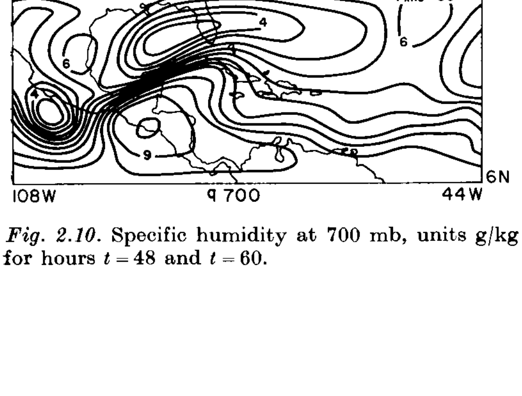

Fig. 2.10. Specific humidity at 700 mb, units g/kg for hours $t = 48$ and $t = 60$.

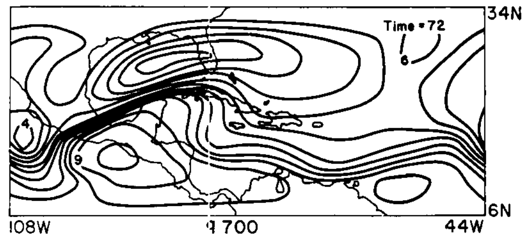

Fig. 2.11. Specific humidity at 700 mb, units g/kg for $t = 72$ hours.

wave and parameterized vertical upward flux of moisture behind the wave axis. Vertical cross sections of specific humidity at 14° N are presented in Fig. 2.12; they show very clearly the steady westward propagation of the dry and moist regions in the experiment. The region of the computed moist front was located close to the region of most active convection; Krishnamurti (1968) noted a similar feature in his observational study. Largest moisture values are found where convection was active in the preceding 12 hours.

Observational evidence of the moisture front from a study of Baumhefner (1968) is shown in Fig. (2.13). The isopleths of relative humidity are portrayed for August 14th 1200Z at 20° N on a vertical cross section. To the west of the 90% relative humidity isopleth the reader may note a sharp gradient and dry air to the west of the easterly wave. Surface weather reports are illustrated at the bottom of this drawing and clouds are schematically illustrated based on the surface reports.

It might have been desirable to construct three dimensional trajectories to examine the change of specific humidity following a parcel. This is not carried out at the present.

(d) *Forecast verification of the large-scale horizontal motion field*

During the first 48 hours of forecast period the tropospheric motion field above the boundary layer (900 mb) was in good agreement with observations. The wave amplitude at 1 000 mb was somewhat lower than what was observed. Figs. 2.14 through 2.16 show the predicted wind field at 200 mb through hour 48. The observed winds are plotted at individual wind observing stations. The wind prediction is in close agreement with observations for the first 36 hours. At 48 hours we note a slight phase

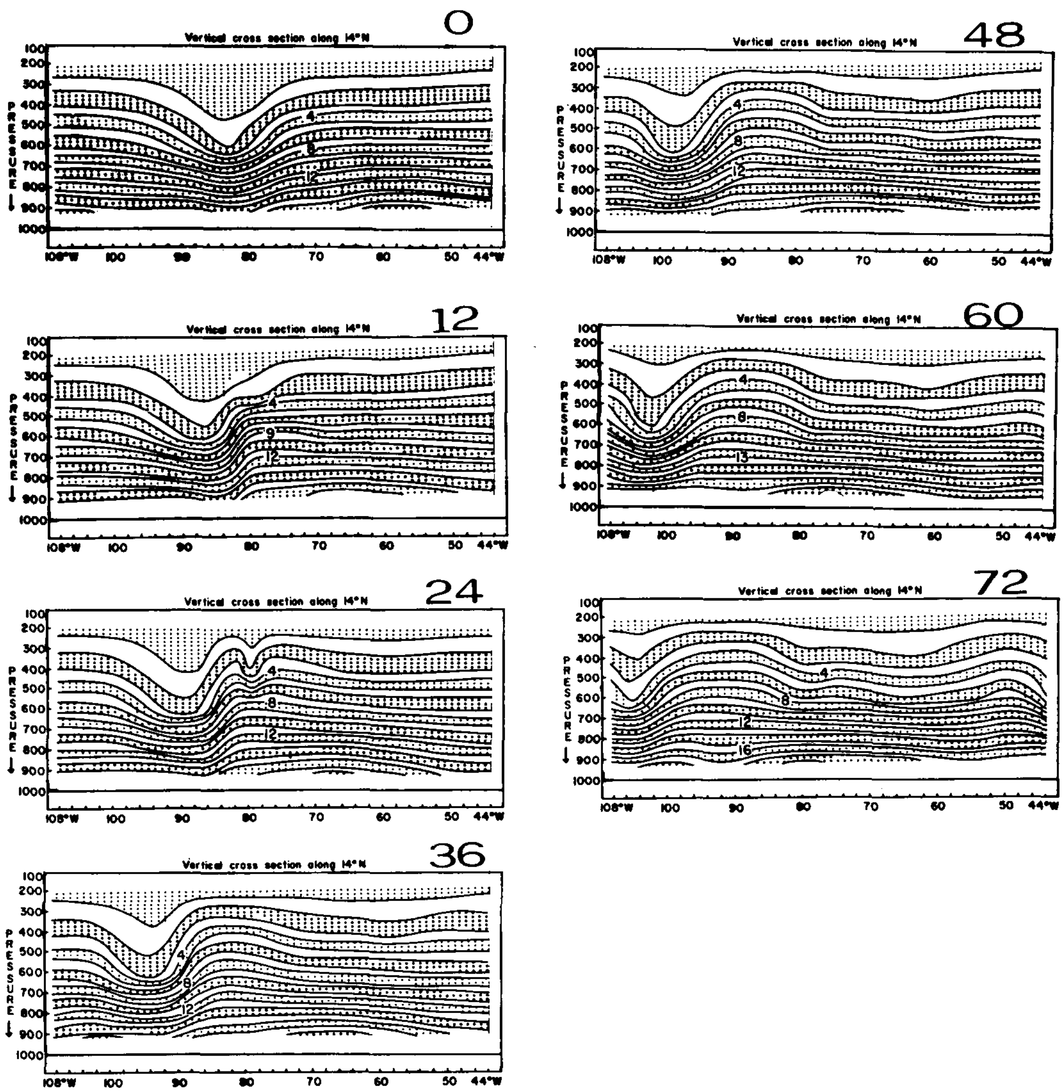

Fig. 2.12. West to east vertical cross section of specific humidity at 14° N latitude. Time between 0 and 72 hours. Shows the westward propagation of the dry and moist regions associated with the wave. Labels on isopleths refer to the mid channel just below the numbers.

lag of the predicted 200 mb motion field. The slow westward motion of the upper low (mid-oceanic trough) was very well predicted by the model. There was, however, a distortion of the mid-oceanic trough near the northern boundary. This is to be expected because of the choice of our boundary conditions. (Please refer to section on boundary conditions in previous paper I). The boundary condition $V = 0$, damp the intensity of the troughs near the Northern boundary.

In Fig. 2.16 we show the 200 mb geopotential height distribution (12 000 meters are to be added to labels on the contours). A comparison of Fig. 2.16 (top and bottom) indicates that the wind and geopotential fields are mutually adjusted to a near quasi-geostrophic equilibrium. Since the domain is north of 6° N the wind-

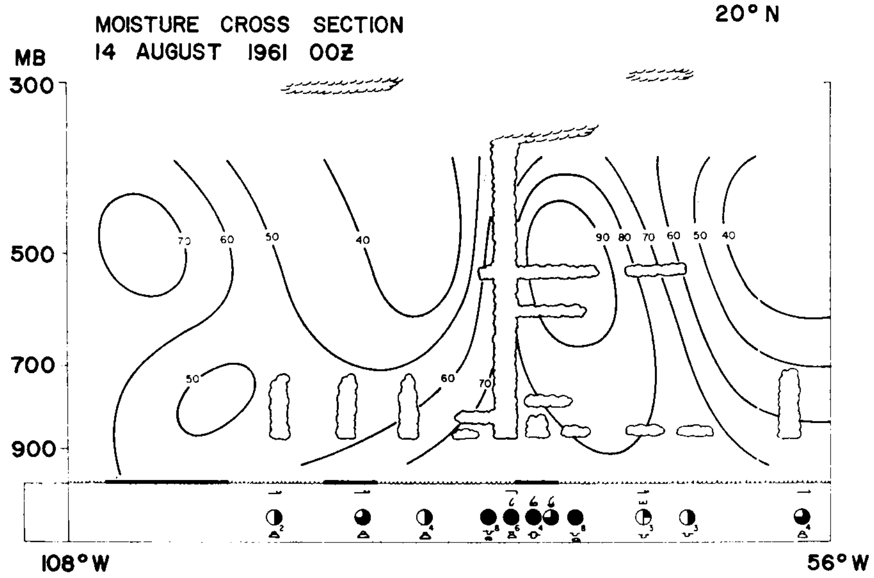

Fig. 2.13. Vertical cross section of relative humidity on Aug. 14, 1961 (from Baumhefner, 1966) at 20° N. Clouds are schematically shown based on surface weather reports indicated at bottom.

height adjustment is not particularly interesting in this study. It should be noted that our initial state did not include the geopotential height distribution as an observed variable. Hence this adjustment of the initialized geopotential during prediction to the motion field is still of considerale importance. The potential of this procedure lies in further applications to very low latitudes where the wind height relationship

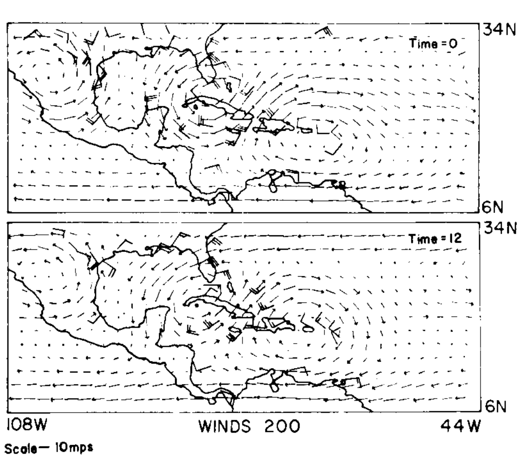

Fig. 2.14. 200 mb wind vectors in the model at hours 0 (initialized) and 12 (forecast). Observed winds (in knots) are plotted at stations.

would be determined via a predictive adjustment.

In our present series of tropical experiments we have accomplished a reasonably stable initialization by following the procedure stated in I. In this problem we have more or less followed the suggestions of Phillips[1] (1960) and have not carried out any further analysis. We do not feel that we have offered a completely satisfactory solution to the tropical initialization problem. It is an important problem and does require separate detailed studies. Our choice of boundary conditions and the quasi-lagrangian advective scheme does seem to yield a rather rapid adjustment of the mass and motion fields. In this process the loss of synoptic-scale information does appear to be minor. For example, at 18 hours the large-scale geometrical features of the distribution of large-scale variables, such as shown in Figs. 2.1, 2.4 does indeed carry most of the geometrical information of the initial state. Unlike an earlier study, Krishnamurti (1969), the present experiment is considerably more stable in this regard. It should however

[1] Phillips showed that if an initial motion field is constructed with a divergent part of the wind field from the so-called 'ω-equation', then the amplitudes of the gravity inertio oscillations are small for a primitive equation prediction model.

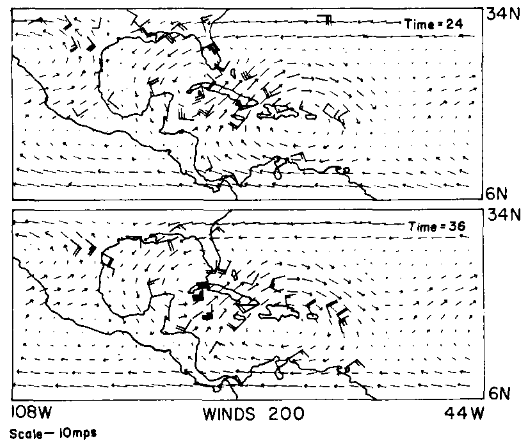

Fig. 2.15. Forecast winds at 200 mb for hours 24 and 36. Observed winds in (knots) are plotted at stations.

be noted that it is the divergent part of the motion field and the geopotential heights at 1 000 mb that seem to exhibit the largest noise during the first 18 hours of adjustment. None of the maps shown in this paper have been smoothed for display purposes.

3. On the restoring of conditional instability

Large-scale tropical soundings, before, during and after disturbance passage exhibit the following characteristics in the lower troposphere,

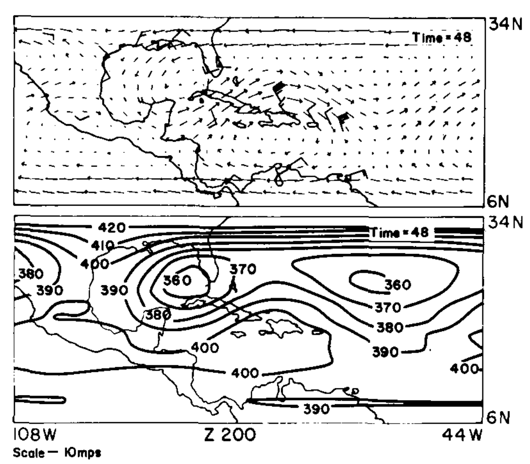

Fig. 2.16. Forecast winds and geopotential heights at 200 mb at $t = 48$ hours. (Add 12 000 to the labels on the lower chart.)

$$-\frac{\partial}{\partial p}(gz + c_p T) > 0 \qquad (3.1)$$

$$-\frac{\partial}{\partial p}(gz + c_p T + Lq) < 0 \qquad (3\text{-}2)$$

The sounding is thus characterized by convective instability. Since the oceanic tropics is usually fairly moist in the boundary layer (i.e., relative humidity usually greater than 80%) if a thin layer of air is lifted upward to saturation, then the above inequalities also may be interpreted as conditional (potential) instability. The maintenance of conditional instability is an important problem in tropical meteorology. Only in the eye wall of the hurricane or in the centers of very tall and large cumulonimbus clouds one encounters undilute ascent (Riehl and Malkus, 1958), and only in these situations we can expect to find

$$-\frac{\partial}{\partial p}(gz + c_p T + Lq) \approx 0$$

Warsh et al. (1971) have examined the Barbados and BOMEX data over the tropical Atlantic during two summer seasons and they note the following interesting properties of the moist static stability in the lower tropopshere.

$$\underset{\text{undisturbed}}{-\frac{\partial}{\partial p}(gz + c_p T + Lq)} < \underset{\text{disturbed}}{-\frac{\partial}{\partial p}(gz + c_p T + Lq)} < 0 \qquad (3.3)$$

They furthermore note that,

$$\left|\frac{\partial}{\partial t}\left\{-\frac{\partial}{\partial p}(gz + c_p T + Lq)\right\}\right|$$

at the time of disturbance passage is much larger than just after disturbance passage. This is to be interpreted as follows: as the disturbance passes over a station conditional instability rapidly changes to a less unstable configuration, while the restoring of the instability is more gradual. The time scales of these are, roughly, 12 hours for a change from very unstable to a less unstable situation and about two days to restore back to the normal unstable configuration. They also note, roughly, a five-day mode in the oscillation of this stability parameter.

A proper specification of the moist static stability of the large-scale tropics is very important for numerical weather prediction. One obvious reason for this being that z, T and q constitute three out of a possible six dependent variables of a primitive equation model. If three of the variables are properly handled then the chances are pretty good that the adjustment of the motion field to the mass field might yield reasonable prediction of most of the other variables. On the other hand, if the moist static stability is not handled properly then the mass field is wrong and the prediction will necessarily be poor. *We have found this to be true from our experience.*

A working equation for the change of moist static stability

The following well-known equation for the heat content per unit mass of air may be used for this purpose,

$$\frac{d}{dt}(gz + c_p T + Lq) = H_s + LE_B + H_R \tag{3.4}$$

Where H_s is the sensible heat transfer from the ocean, LE_B is the latent heat transfer and H_R is the rate of radiative warming. Some approximations are made in deriving the above equation such as neglect of orizontal kinetic energy, its dissipation, and terms of the same order of magnitude. In a closed system, in the absence of heat sources and sinks the net heat content over the domain will be an invariant.

If we let $E_m = gz + c_p T + Lq$ we may write equation (3.4) in the form,

$$\frac{\partial}{\partial t} E_m = -\mathbf{V} \cdot \nabla E_m - \omega \frac{\partial}{\partial p} E_m + H_s + LE_B + H_R \tag{3.5}$$

Next we shall define bar and prime, where bar will denote grid scale (resolvable scale) variable, and prime the subgrid scale motions. From equation (3.5) we obtain,

$$\frac{\partial}{\partial t} \bar{E}_m = -\bar{\mathbf{V}} \cdot \nabla \bar{E}_m - \bar{\omega} \frac{\partial}{\partial p} \bar{E}_m - \frac{\partial}{\partial p} \overline{\omega' E_m'} + \bar{H}_s + \overline{LE}_B + \bar{H}_R \tag{3.6}$$

Horizontal convergence of flux of E_m by eddies is neglected in the above relation, the underlying assumption here being that the vertical eddy flux is more important.

If we differentiate (3.6) with respect to presure and let

$$\bar{\Gamma}_m \text{ (moist static stability of large-scale flow)} = -\frac{\partial}{\partial p}(g\bar{z} + c_p \bar{T} + L\bar{q}) \tag{3.7}$$

then we obtain,

$$\frac{\partial \bar{\Gamma}_m}{\partial t} = -\bar{V} \cdot \nabla \bar{\Gamma}_m - \bar{\omega} \frac{\partial}{\partial p} \bar{\Gamma}_m + \frac{\partial^2}{\partial p^2} \overline{\omega' E_m'} - \bar{\Gamma}_m \frac{\partial \bar{\omega}}{\partial p} - \frac{\partial \bar{H}_s}{\partial p} - L \frac{\partial}{\partial p} \bar{E}_B - \frac{\partial \bar{H}_R}{\partial p} \tag{3.8}$$

Equation (3.8) is our working equation for the local change of moist static stability. It should be noted that in the absence of heat sources, sinks and smaller scale eddy motions the net large-scale moist static stability over a closed domain is not an invariant. Large-scale subsidence or convergence can alter the stability via term 4 on the right-hand side. The following interpretation of individual terms on the right-hand side of equation (3.8) may be of interest. Terms 1 and 2 essentially are results of large-scale advection of moist static stability in the horizontal and vertical directions, respectively. Term 3 shows that the vertical profile of the eddy flux of moist static energy E_m' can play a role in the stabilizing and destabilizing process. Warsh et al. (1971) suggest that, of these the vertical eddy flux of moisture, $\overline{\omega' q'}$, is the most important part of $\overline{\omega' E'}$ during disturbance passage. Although we agree with that in principle, we find that $\omega' T'$ in disturbed areas can also contribute significantly to the stabilizing of the moist static instability of the lower tropical troposphere. Term 4 denotes the effects of large-scale convergence and divergence on the large-scale moist static stability. The so-called subsidence inversion usually forms in regions where this term is large, Lahiff (1971). Large-scale divergence has a stabilizing effect.

Subsidence tends to increase (i.e. more positive) the dry static stability i.e. $-\partial/\partial p(g\bar{z} + c_p \bar{T})$ and in these regions the value of $-\partial/\partial p(g\bar{z} + c_p \bar{T} + L\bar{q})$ is also noted to decrease (i.e. becomes more negative).

Terms 5 and 6 relate to air-sea interaction and if $\bar{H}_s$ and LE_B are positive then these effects would result in a distabilization at lower levels.

Term 7 refers to radiative cooling. Cooling at cloud top levels would result in destablization on a restoring of the conditional instability. Lilly (1970) has discussed the formation of the marine inversion in this context.

It might have been desirable to study the variation of moist static stability along trajectories, due to strong vertical shears and attendant difficulties which is not carried out here.

In the following we shall examine the results at a grid point during a 72-hour period of numerical prediction. The active portion of the wave passes over this grid point. The computations refer to the layer between 900 and 700 mb. Table 2 shows the various terms in three hourly intervals, units of each term are expressed in $m^2\ sec^{-3}\ mb^{-1}$. Prior to the active disturbance passage at $t = 3$ hr the local change of moist static stability is primarily due to large-scale advective processes.

During the passage of the active portion of the wave, $t \approx 27$ hr, vertical eddy flux of moisture dominates the stabilizing effects. The vertical eddy flux of sensible heat is about half as large as the effect of vertical eddy flux of moisture. It should be noted that these vertical eddy flux terms are evaluated on the basis of the parameterization procedure that is used for these forecasts, i.e.

$$-\frac{\partial}{\partial p}\overline{\omega' q'} = \frac{a(q_s - q)}{\Delta \tau} \tag{3.9}$$

and

$$-\frac{\partial}{\partial p}\overline{\omega' T'} = \frac{a(T_s - T)}{\Delta \tau} \tag{3.10}$$

In equation (3.9) and (3.10) the left hand side denotes vertical convergence of eddy flux of moisture and temperature respectively. The right hand side represents the parameterication used in I, i.e. Krishnamurti et al. (1973). 'a' is the fraction area of a cloud cover, $\Delta\tau$ is a cloud time scale, T_s and q_s refer respectively to temperature and specific humidity for a reference moist adiabat and T and q are corresponding ambient temperature and specific humidity. In general we note that the instantaneous effects of air-sea interaction and of radiation are much smaller than the convective transports at this stage.

After disturbance passage (at 72 hours) conditional instability is slowly restored by horizontal advective processes, air-sea interaction and by radiation. Horizontal advection is large throughout the 72 hours because the wind speed in the lower troposphere is somewhat larger than the wave speed.

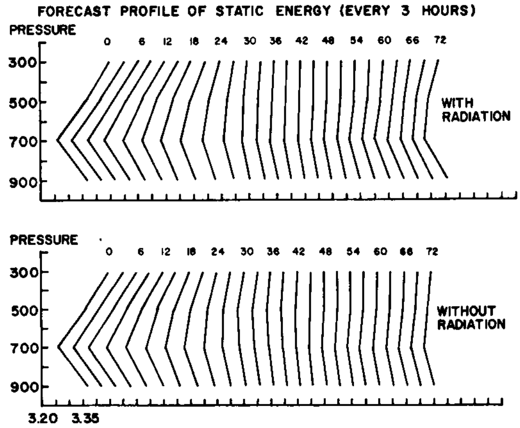

Fig. 3.1. Three hourly vertical profiles of moist static energy at a grid point illustrating the effect of wave passage. The horizontal scale for time $t = 0$, bottom left, refers to $3.20 \times 10^5\ m^2\ sec^{-2}$ This scale should be moved to the right by one division per 3 hours.

Fig. (3.1) shows the time evolution of the vertical profile of moist static energy in three hourly intervals for the same grid point. This includes the results of two experiments, one forecast with radiative effects and the other without these effects. Of interest to note here is the marked restoring of the conditional instability after disturbance passage when radiation is included. During disturbance passage the vertical slope of the static energy lines is very small. It appears that the radiative effect is small in the instantaneous picture, but its integrated influence over 72 hours is significant.

Radiative effects of our model are discussed in a detailed section of I. Explicit calculations of cooling rates are evaluated as a function of evolving temperature, moisture and cloud criteria. The net radiative flux is evaluated using three considerations at any level:

i) black body flux from cloud layers above and below the level,
(ii) emissions by cloud free regions above and below the level,
(iii) absorption of long wave radiation by cloud

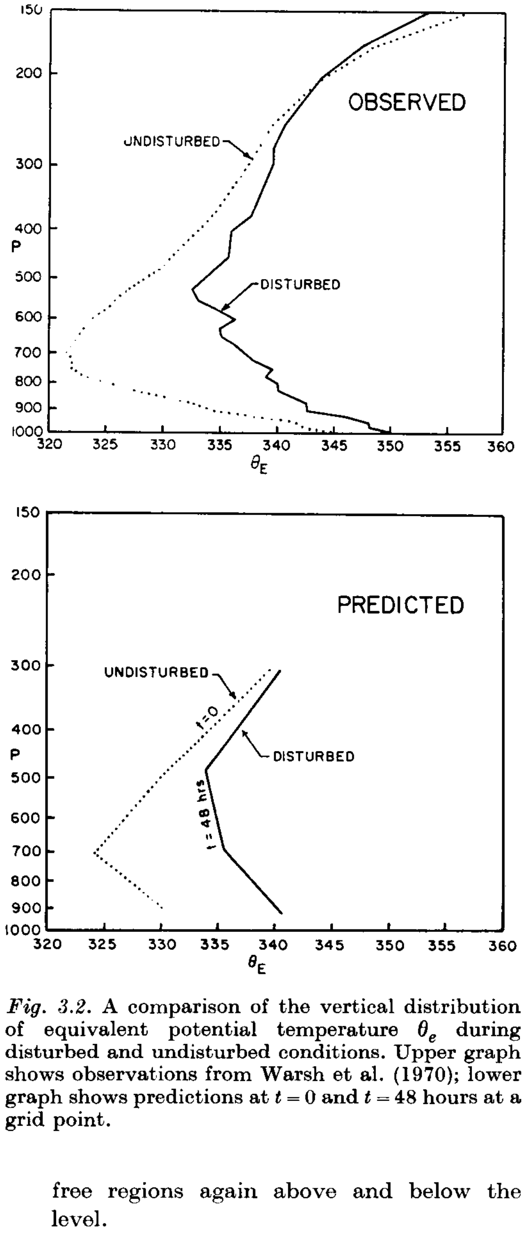

Fig. 3.2. A comparison of the vertical distribution of equivalent potential temperature θ_e during disturbed and undisturbed conditions. Upper graph shows observations from Warsh et al. (1970); lower graph shows predictions at $t = 0$ and $t = 48$ hours at a grid point.

free regions again above and below the level.

The following further results of these calculations are of interest. Around the disturbed (convective) region radiative cooling rates in the middle and lower troposphere (near 700 mb) are larger than inside the disturbed areas. Downward motions around the disturbed areas are enhanced by the inclusion of radiative cooling. An approximate balance between adiabatic warming in this descending region and the radiative cooling is realized. The moist layer around the disturbance is found to be gradually lowered by this subsidence. The cooling rates are usually large just above the moist layer. Thus around the disturbance θ_e-minimum values are generated near the 700 mb surface due to two factors: (i) drying, i.e. lower values of q in subsiding regions, and (ii) cooling (lower θ values) on the top of the moist layer. We feel that over large-scale tropics a marked restoring of conditional instability is in effect brought out in the regions around the disturbed areas.

Fig. 3.2 shows a comparison of observed versus computed changes of the θ_e profiles between undisturbed versus disturbed conditions. The observations are based on the studies of Warsh et al. (1970) and the computations for the present experiment include the radiative effects.

We conclude this section with the remark that a somewhat realistic prediction of the moist static stability and the problem of the restoring of the conditional instability is possible with the kind of physics that we have used in the present model.

There are however several limitations of the present work that may be noted. We are not able to reproduce in exact detail time sections of the moist static energy profiles over many stations in our network. We find also that although the slope of the θ_e profiles are somewhat realistic the individual values, especially at 900 mb, are somewhat too large. Some of this, we feel, may be due to the crudeness of our radiative cooling calculations.

4, On the maintenance of the cold low

Fig. 4.1 through Fig. 4.4 shows the potential temperature field at 900 mb in 12 hourly intervals from time $t = 0$ to time $t = 72$ hours. The potential temperature isopleths at 900 mb can also be regarded as isotherms on the 900-mb surface. Of particular interest in this sequence of diagrams is the westward propagation of the cold core of the easterly waves. The initial potential temperature in the wave, marked with the letter C, is around 300°K. As the wave propagates from east to west, during the course of 72 hours we notice that the temperature of the cold core is maintained within 1 or 2°C during the entire course of the integration.

Table 2. *Terms of moist static stability equation, 800 MB, units in 10^{-5}* m² sec⁻³ mb⁻¹

Time in hours	0	3	6	9	12	15	18	21	24	27	30	33
$\frac{\partial \overline{\Gamma m}}{t}$		28.3	36.6	48.1	48.9	41.8	34.2	34.5	42.1	43.5	21.9	2.3
$-\bar{\omega}\frac{\partial}{\partial p}\overline{\Gamma}_m$		22.3	4.6	5.7	15.7	6.0	0.3	−6.6	−12.8	−5.2	−3.6	−3.0
$-\bar{\mathbf{v}}\cdot\nabla\overline{\Gamma}_m$		13.8	22.3	21.2	25.0	24.6	15.9	15.8	20.8	20.3	21.7	18.2
$-\frac{\partial\bar{\omega}}{\partial p}\overline{\Gamma_m}$		−6.2	5.1	1.2	−1.9	−3.2	−5.8	−4.3	2.3	3.3	4.5	4.6
$\frac{\partial^2}{\partial p^2}\overline{L\omega' q'}$		0.0	0.0	0.0	0.1	3.0	9.2	22.6	46.1	63.2	51.8	39.4
$\frac{\partial^2}{\partial p^2}c_p\overline{\omega' T'}$		0.0	0.0	0.0	0.0	1.5	5.2	12.2	23.5	30.8	27.8	23.1
$-\frac{\partial \bar{H}_R}{\partial p}$		−3.1	−2.8	−3.7	−4.5	−4.7	−4.8	−4.7	−4.6	−4.8	−5.5	−6.2
$-\frac{\partial}{\partial p}(\bar{H}+L\bar{E}_s)$		−6.1	−5.5	−5.5	−5.3	−5.1	−4.7	−4.8	−5.7	−6.3	−6.0	−4.9

The temperature change is indeed very small, and the coasting easterly wave does maintain a thermal structure in near steady state. This is extremely gratifying from the point of view of numerical weather prediction, because in order to carry out a numerical experiment where the temperature changes are to be maintained within a degree or so in the presence of air-sea interaction, deep convection and radiation requires a fairly sophisticated model which is sensitive enough to yield such results.

It should be noted that the model is found to be quite sensitive to radiative cooling, air-sea interactions and cumulus convection. Considerable care was exercised in selecting a reasonable formulation of these and we feel that these results are quite representative.

Although temperature gradients weaken some-

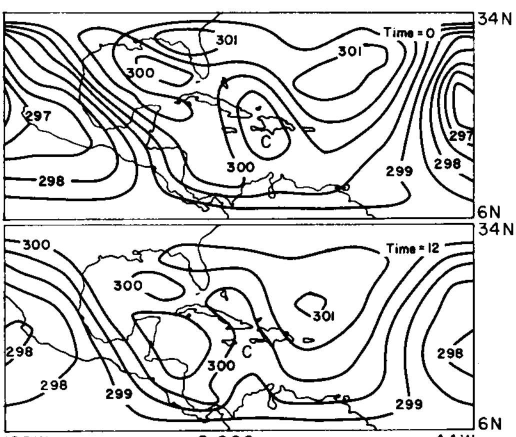

Fig. 4.1. Potential temperature, θ, at 900 mb. Interval 0.5°C. $t=0$ and $t=12$ hours.

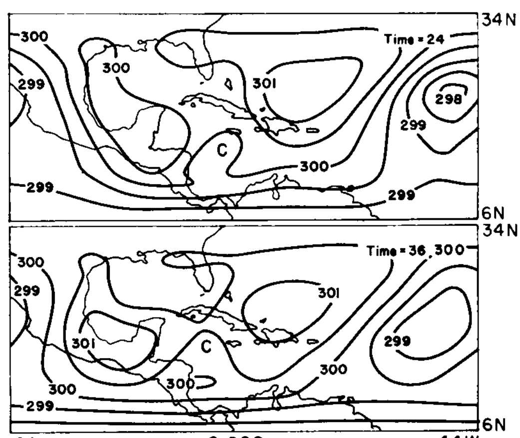

Fig. 4. 2. Potential temperature, θ, at 900 mb. Interavl 0.5°C. $t=24$ and $t=36$ hours.

36	39	42	45	48	51	54	57	60	63	66	69	72
8.4	15.0	2.7	−13.6	−19.3	−25.3	−31.3	−34.7	−23.4	−26.5	−28.1	−40.5	−45.9
−2.6	−2.3	−2.5	−3.3	−3.9	−6.4	−8.6	−8.3	−8.3	−6.0	−1.3	1.8	−0.2
13.2	15.1	6.7	−6.9	−12.6	−16.8	−21.8	−22.9	−20.0	−18.3	−19.3	−23.4	−29.1
2.4	1.1	1.2	2.6	3.3	5.3	7.7	9.3	10.4	8.2	2.6	−2.7	−4.0
0.0	33.5	0.0	0.0	0.0	0.0	0.0	0.6	0.0	26.7	12.5	3.7	0.0
19.8	19.6	19.6	23.1	26.7	28.8	32.8	31.4	25.7	17.1	8.4	2.3	0.0
−6.0	−6.1	−6.3	−6.6	−6.4	−6.0	−5.6	−5.0	−4.4	−3.8	−3.2	−2.9	−2.6
−4.2	−4.4	−4.6	−4.9	−5.1	−5.1	−5.3	−5.4	−5.0	−4.5	−3.8	−3.4	−3.2

what in the initial 12 hours, thereafter gradients are very well preserved. We feel that the initial period of the first 12 hours or even up to the first 18 hours is a period of adjustment and during this time considerable changes in the initial input field do take place. Nevertheless, one could note that the temperature distribution in the vicinity of the cold core wave is not altered very much and this is primarily the region of interest of this study. An important question that does arise in the context of the results presented in these diagrams is that of the maintenance of the cold core easterly wave in near steady state. The experiment was repeated without convection and we noted that the cold core weakened within 36 hours. Only in the experiments including convection the cold core could be maintained. In the experiment without radiation temperature gradients were somewhat larger than the experiment with radiation, although the intensity of the cold core is about the same in both of these experiments. Cold core easterly wave, we found, was maintained primarily by ascending motions in the region of the boundary layer of the active portion of the

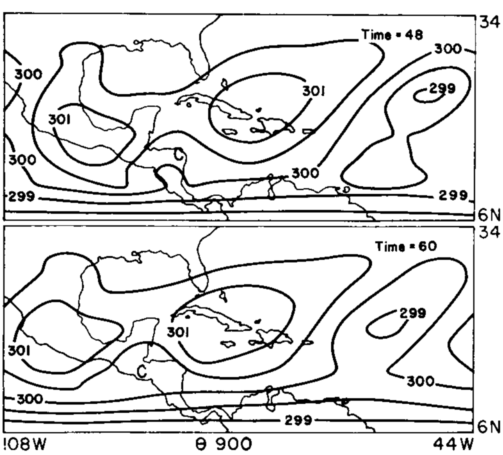

Fig. 4.3. Potential temperature, θ, at 900 mb. Interval 0.5°C. $t = 48$ and $t = 60$ hours.

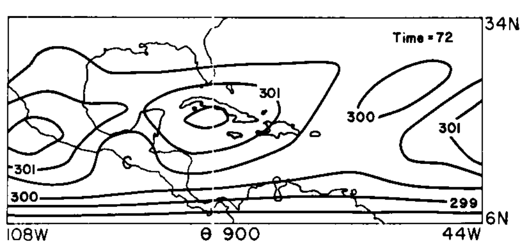

Fig. 4.4. Potential temperature, θ, at 900 mb. Interval 0.5°C. $t = 72$ hours. Figs. 4.1 through 4.4 illustrate the westward propagation of the cold low.

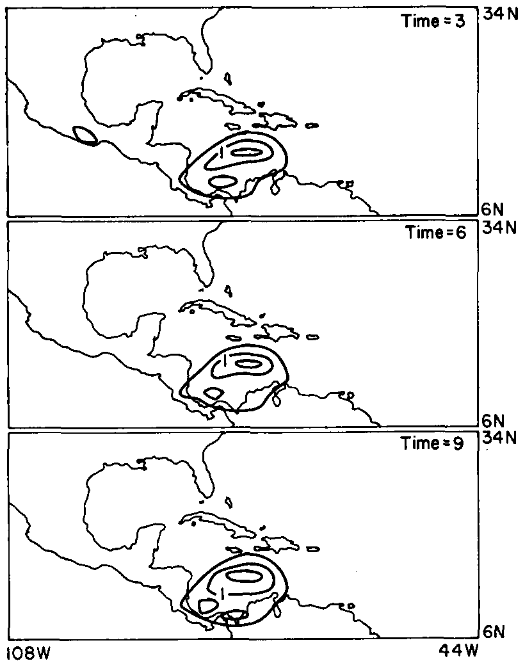

Fig. 5.1. Fraction area (percent of grid scale area) of deep convection at hours $t = 3$, 6 and 9 hours.

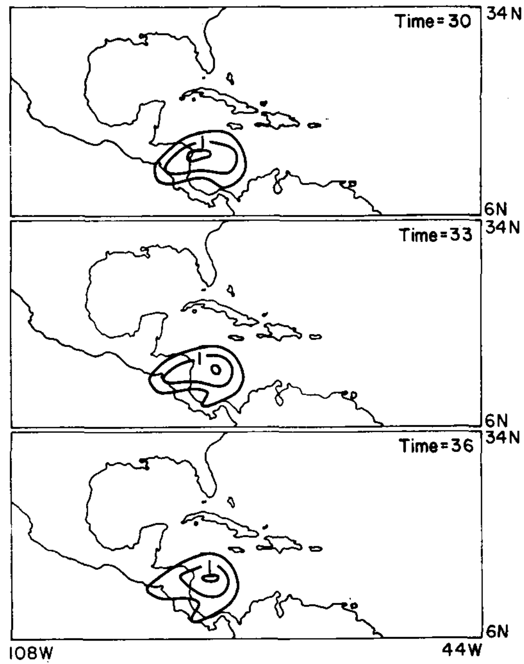

Fig. 5. 2. Fraction area (percent of grid scale area) of deep convection at hours $t = 30$, 33 and 36 hours.

wave. Ascending motions account for adiabatic cooling and they arise due to frictional convergence and heating aloft above the cold core of the wave where the cumulus-scale convection is parameterized. There is an effective net heat release on top of the cold core. Indeed there does exist a warm core above the cold core, this can be seen in the temperature field above 700 mb. The intensity of this warm core is also of the order of a couple of degrees centigrade and is not very pronounced.

The cold core is not merely an advective phenomena that translates from east to west but is maintained by dynamic and thermodynamic processes. This point will be stressed further later on in the discussion of the energetics and on the discussion of the parameterization as to what it can and cannot do in the context of the present model. It should be noted that the 900-mb surface is the lifting condensation level and at that level the difference between the temperature of the moist adiabat and the environment is assumed to be zero. There is no explicit region where this temperature difference between the moist adiabat and that of the environment is negative, although an extrapolation below 900 mb would define an implicit region where the ascending parcels would encounter a negative temperature difference between that of the moist adiabat and the environment. So, in some sense the formation of the cold core due to adiabatic rising motions is also somewhat analogous to that of the tropical cold core disturbances that were found by Manabe et al. (1970) in their general circulation studies over the tropics.

Although observational studies have well documented the upper warm core structure of cold core lower tropospheric waves, the present studies merely point out some of the complex difficulties one faces in the numerical simulations of such.

5. Statistical equilibrium of the area occupied by deep convection

As stated in I the fraction of the grid-scale area covered by deep convection is expressed by the parameter a.

Figs. 5.1 through 5.3 show a sequence of selected drawings, starting from hour 3 through

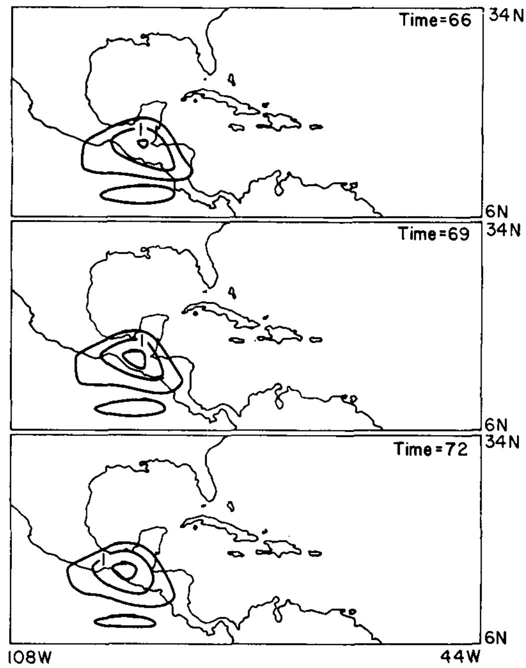

Fig. 5.3. Fraction area (percent of grid scale area) of deep convection at hours $t = 66$, 69 and 72 hours.

hour 72, of the fraction area of computed cloud cover. Of interest here is the statistical steadiness of the fraction area of the convection. We note in these computations that 1 to 1 1/2% of the 2° latitude by 2° longitude squares of the mesh size is covered by deep convection. This region of deep convection proceeds westward with the easterly wave, the region of maximum cloud cover being located just to the east of the surface wave axis. This computation is also very gratifying from the point of view that there is indeed a statistical equilibrium of the cumulus scale as prescribed by the parameterization procedure; the near steady state of the fraction area is found to be in a cooperative equilibrium with the large-scale coasting easterly wave. Over this region of 1% cover there is ascending motion on the large scale, this results in cooling at lower levels and a release of latent heat and warming at higher levels. In other studies, where the initial states are different, we find that the field of "a" can change markedly. In the developing hurricane it increases rapidly, while in the study of a decaying wave it is found to decrease with time. We feel that the reasons for the statistical equilibrium of cloud cover cannot be discussed without reference to the overall energetics of the disturbance.

6. On the energetics of the wave

The rate of increase of eddy kinetic energy in a closed domain may be expressed, following Lorenz (1967), by the relation,

$$\frac{\partial K'}{\partial t} = -\int_M \left\{[u'v]\frac{\partial}{\partial y}[u] + [u'\omega']\frac{\partial}{\partial p}[u] + [v'v']\frac{\partial}{\partial y}[v] + [v'\omega']\frac{\partial}{\partial p}[v]dM\right\} - R\int_M \frac{[\omega'T']}{p}dM - \int_M \{[u'F_x'] + v'F_y']\}dM \qquad (6.1)$$

Here M stands for the mass of the domain, [] stands for a zonal average and primes denote a departure from a zonal average, F_x and F_y are frictional forces along the zonal and meridional direction per unit mass of air. The remaining symbols are the same as in I. For convenience we may write the three integrals on the right-hand side of Eq. (6.1) by new symbols.

$$\frac{\partial K'}{\partial t} = \langle K_z K_E\rangle + \langle P_E K_E\rangle + D' \qquad (6.2)$$

where $\langle K_Z K_E\rangle$ denotes barotropic energy exchanges, $\langle P_E K_E\rangle$ denotes baroclinic energy exchanges, and D' denotes dissipation of eddy kinetic energy in the domain.

The maintenance of a tropical cold core easterly wave is usually considered as somewhat of an enigma, Charney & Eliassen (1964). Barotropic instability has been shown as an important energy source for the formation of these waves over western Pacific, Yanai & Nitta (1968).

Along these considerations one might speculate that the wave receives energy from the horizontal shear flows and loses energy due to the general ascent of relatively cold air and due to frictional dissipation, i.e. $\langle K_Z K_E\rangle > 0$, $\langle P_E K_E\rangle < 0$ and $D' < 0$. Our computations cover a band of latitude circles that enclose an active part of the wave, however yields a different result.

Fig. 6.1 shows the results of computations (after 18 hrs) of the two principal energy ex-

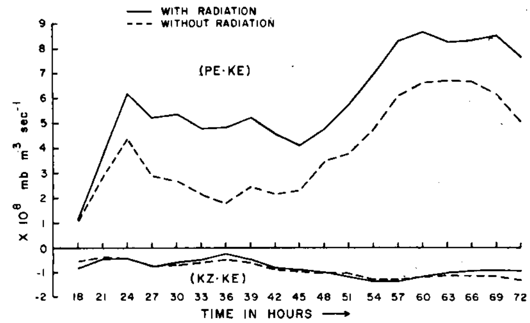

Fig. 6.1. Barotropic and baroclinic energy exchanges between 18 hours and 72 hours for two experiments, with and without long-wave radiative cooling effects. The energy exchange are evaluated using Eq. 6.1 for a latitude belt 12° wide across the active part of the wave and between 100 and 1 000 mb surfaces.

changes. The first 18 hrs are regarded as model adjustment time. The computations include results from two different experiments, those carried out with and without radiative effects. The wave loses energy to the mean zonal flows, i.e. $\langle K K_E \rangle$ is <0, and is maintained by the energy conversion $\langle P_E K_E \rangle > 0$. The latter results from warmer air rising above the cold low. This ascending motion of warmer air is primarily due to latent heat release. Ceselski (1972) has noted that the cold and warm cores in this disturbance cannot be maintained without the parameterization of cumulus convection. Thus we view our results of the energetics as follows: parameterized cumulus scale motions provide

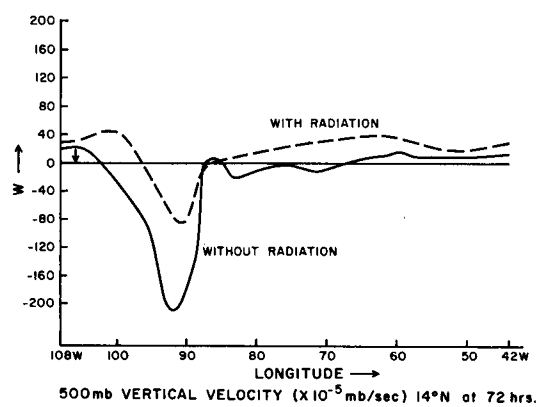

Fig. 6.2. Differences in vertical velocity, ω, at 500 mb in two experiments at 72 hours. Note the larger subsidence both east and west of the rising region where long-wave radiative cooling is included.

an important mechanism for the generation of eddy kinetic energy, $\langle P_E K_E \rangle > 0$, and thus the cumulus scale is crucial for the maintenance of this wave.

As regards radiation, in section 3, we noted that the inclusion of cooling by long-wave radiative effects tends to enhance the intensity of sinking motion around the wave, see Fig. 6.2.

Thus we note that, Fig. 6.1,

$$\underset{\text{with radiation}}{\langle P_E K_E \rangle} > \underset{\text{without radiation}}{\langle P_E K_E} > 0 \qquad (6.3)$$

Thus differential radiative cooling appears to be important in short range numerical weather predictions over the tropics. It should be noted that over middle latitudes in an extratropical cyclone the intensity of large-scale vertical motion is usually of the order of 10 cm/sec and the inclusion of long-wave radiative effects tends to alter this by about 10% (Danard, 1969). However over the tropics a change in vertical motion of around 1 cm/sec is a large proportion of the total large-scale vertical motion, and thus a sizeable difference in the correlation $\overline{\omega' T'}$ may be noted.

A complete evaluation of the energetics of an open system is presently being examined, these results will be published at a later date.

7. Concluding remarks

The vertical distribution of heating in our present series of experiments is proportional to $(T_s - T)$. It should be noted that the present trend of (unpublished) research on the problem of parameterization of cumulus convection is toward inclusion of explicit downdraft mechanisms, evaporation of liquid water and falling rain, entrainment and detrainment processes in clouds. A sophistication of this size would certainly be desirable for at least the following two reasons: First, to obtain a clearer physical rationale for the parameterization of cumulus convection, and secondly for possible improvement in the state of numerical weather prediction, especially over the tropics.

Our present scheme of parameterization of cumulus convection is an extension of the original proposition of Kuo (1965). It invokes the principle of conservation of moist static energy. Implicitly it does invoke strong updrafts and (for mass balance) downdrafts. This is evidenced by the fact that the vertical eddy flux of moisture, implied by our procedure, does transport moisture up from the boundary layer at a rate much faster than is implied by large-scale upward vertical velocity, Krishnamurti & Hawkins (1970). If we regard the large-scale net moist static energy convergence to be prescribed as one major constraint, then we might perhaps rationalize the use of $(T_s - T)$, for the vertical distribution of heating, on the following grounds

(*a*) We assume that on the cumulus scale all of the upward flux of moisture takes place in the region of updrafts only. Over the region of downdrafts, the drying by subsidence is exactly compensated by evaporation of liquid water from the sides of the cloud. Under these assumptions the vertical distribution of moisture would be proportional to $(q_s - q)$.

(*b*) The question we next ask is for a given total static energy convergence, what are some of the possible realizations of the vertical distributions of T and Z?

(*c*) Since the final vertical distribution of T and Z are constrained to be in hydrostatic equilibrium we are thus only concerned with determining the final vertical distribution of one of these variables, let us say T.

(*d*) It is clear that for energetic consistency, a vertical distribution of heating proportional to $(T_s - T)$ is definitely one of the solutions that satisfies our problem.

At this stage we are not able to prove that this would be unique in any manner. In this paper we have essentially shown the practical validity of such a simple vertical variation of heating for 3-day integrations. Others who have successfully used this type of simple scheme on tropical problems are:

Yamasaki (1968)	symmetric hurricane idealized initial state
Rosenthal (1970)	symmetric hurricane idealized initial state
Sundquist (1970)	symmetric hurricane idealized initial state
Anthes et al. (1971)	asymmetric hurricane idealized symmetric initial state
Mathur (1972)	asymmetric hurricane with real data

In view of above successes, we feel that further theoretical analysis of this type of heating function would be deirable.

In this paper we have shown that a somewhat reasonable prediction of the mass, motion and moisture variables for periods of 2 to 3 days is possible. We find that it is possible to maintain the cold core of the easterly wave primarily from rising motions in the disturbed areas. The intensity of the rising motion is enhanced by the inclusion of cumulus scale heating aloft; thus the latter is found to be crucial for the maintenance of the lower tropospheric cold low. Furthermore we found that radiative cooling around the disturbed regions are somewhat larger than in the disturbed areas. Convergene of flux of this air into the disturbed areas also contributes significantly toward the maintenance of the cold core. Differential radiative cooling is also shown to have an important role in the restoring of the large-scale conditional instability of the tropics. Over the disturbed region convective processes are shown to stabilize the vertical profile of moist static energy. We find that it is the region around the disturbance where the largest restoring of the conditional instability takes place. (In the preceding discussion we have used the term disturbed area to imply that region where convective heating is released in the vertical.) As regards the energetics of the wave we find that the major energy source for the wave arises from the parameterized cumulus scale motions and not the horizontal shear of the mean zonal flow. Throughout the 72-hour period the latter is found to be an energy sink for the disturbance.

There are several limitations of the present work. A clear physical understanding of the heating function is presently lacking. The model produces a slight warming of the θ_e values at 900 mb. This may be due to improper coupling of the air-sea interactions and radiative effects. Better data is needed for both initialization and verification. Hopefully for the coming GARP Atlantic Tropical Experiment (GATE) we shall be able to extend our studies into more fruitful investigations.

8. Acknowledgements

This work was supported by the atmospheric sciences section of the National Science Foundation under Grant No. GA17822 and by the Department of Defense Grant No. DAAB-07-68-

COO62. Computation time was provided by the Computing Facility of the Florida State University (CDC 6400) and by the National Center for Atmospheric Research (CDC 6600, CDC 7600) which again is supported by the National Science Foundation.

REFERENCES

Anthes, R. A., Rosenthal, S. L. & Trout, J. W. 1971. Preliminary results from an asymmetric model of the tropical cyclone. *Mon. Wea. Rev. 99*, 744–758.

Baumhefner, D. P. 1968. Application of a diagnostic numerical model to the tropical atmosphere. *Mon. Wea. Rev. 96*, 218–228.

Ceselski, B. 1972. A comparison of cumulus parameterization techniques in numerical integrations of an easterly wave. Ph.D. Dissertation, Department of Meteorology, Florida State University, Tallahassee, 97 pp.

Charney, J. G. & Eliassen, A. 1964. On the growth of the hurricane depression. *J. Atm. Sci. 21*, 68–75.

Danard, M. B. 1969. A simple model of including longwave radiation in a tropospheric numerical prediction model. *Mon. Wea. Rev. 97*, 77–85.

Krishnamurti, T. N. 1968. A diagnostic balance model for studies of weather systems of high and low latitudes, Rossby number <1. *Mon. Wea. Rev. 96*, 197–207.

Krishnamurti, T. N. & Hawkins, R. S. 1970. Midtropospheric cyclones of the southwest monsoon. *J. Appl. Meteor. 9*, 442–458.

Krishnamurti, T. N., Kanamitsu, M., Ceselski, B. & Mathur, M. 1973. Florida State University's tropical prediction model. *Tellus 25*, 523–535.

Kuo, H. L. 1965. On formation and intensification of tropical cyclones through latent heat release by cumulus convection. *J. Atmos. Sci. 22*, 40–63.

Lahiff, L. N. 1971. A numerical study of a subtropical marine stable layer. Ph.D. Dissertation, Florida State University, Tallahassee.

Lilly, D. K. 1968. Models of cloud topped mixed layers under strong inversion. *Quart J. Roy. Meteor. Soc. 94*, 292–309.

Lorenz, E. N. 1967. The nature and theory of the general circulation of the atmosphere. Geneva, World Meteorological Organization, pp. 1–161.

Manabe, S., Holloway, J. L., Jr and Stone, H. M. 1970. Tropical circulation in a time integration of a global model of the atmosphere. *J. Atmos. Sci. 27*, 580–613.

Mathur, M. B. 1972. Simulation of an asymmetric hurricane with a fine mesh multiple grid primitive equation model. Ph.D. Dissertation, Florida State University, Tallahassee.

Phillips, N. A. 1960. On the problem of initial data for primitive equations. *Tellus 12*, 121–126.

Riehl, H. & Malkus, J. S. 1958. On the heat balance in the equatorial trough zone. *Geophysica 6*, 503–538.

Rosenthal, S. L. 1970. A circularly symmetric primitive equation model of tropical cyclone development containing an explicit water vapor cycle. *Mon. Wea. Rev. 98*, 643–663.

Sundquist, H. 1970. Numerical simulation of the development of tropical cyclones with a ten-level model, Pt. I. *Tellus 22*, 359–390.

Warsh, K. L., Echternacht, K. L. & Garstang, M. 1971. Structure of near surface currents east of Barbados. *J. Phys. Oceanogr. 1*, 123–129.

Yamasaki, M. 1968. Detailed analysis of a tropical cyclone simulated with a 13-layer model. *Papers in Meteor. and Geophys. 19*, 559–586.

Yanai, M. & Nitta, T. 1968. Finite difference approximations for the barotropic instability problem. *J. Meteor. Soc. Japan 46*, 389–403.

ИЗУЧЕНИЕ ВОСТОЧНОЙ ВОЛНЫ

Представлены результаты использования многоуровенной модели, основывающейся на использовании примитивных уравнений. Физика модели включает в себя взаимодействие атмосферы и океана, мелкую и глубокую влажную конвекцию и эффекты длинноволновой радиации. В статье представлен пример прогноза для неразвивающейся волны, распространяющейся с востока на запад. Показано, что можно получить разумный прогноз движения и интенсивности волны до периодов порядка 72 часов. Расчеты расширены для изучения ряда важных проблем, имеющих сюда отношение, таких как: 1. Поддержание и энергетика холодного ядра возмущения; 2. Восстанавливающий механизм, действующий на крупномасштабную условную неустойчивость тропической атмосферы во время и после прохождения возмущения; 3. Эффекты дифференциальности длинноволновой радиации на прогноз; 4. Статистическое равновесие области параметризованных движений масштаба кучевых облаков в зависимости от движений большего масштаба; 5. Важность простой процедуры параметризации для краткосрочного прогноза погоды.